REFRACTIVE INDEX CHARACTERIZATION OF FIBER SENSOR

WOON SIN LING

A project report submitted in partial fulfilment of the requirements for the award of Bachelor of Science (Hons.) Physics

Lee Kong Chian Faculty of Engineering and Science
Universiti Tunku Abdul Rahman

September 2015

DECLARATION

I hereby declare that this project report is based on my original work except for citations and quotations which have been duly acknowledged. I also declare that it has not been previously and concurrently submitted for any other degree or award at UTAR or other institutions.

Signature : _____

Name : Woon Sin Ling

ID No. : 1106271

Date : _____

APPROVAL FOR SUBMISSION

I certify that this project report entitled **"REFRACTIVE INDEX CHARACTERIZATION OF FIBER SENSOR"** was prepared by **WOON SIN LING** has met the required standard for submission in partial fulfilment of the requirements for the award of Bachelor of Science (Hons.) Physics at Universiti Tunku Abdul Rahman.

Approved by,

Signature : _____

Supervisor : Mr. Lin Horng Sheng

Date : _____

Dedicated to Elias, my son

ACKNOWLEDGEMENTS

Much appreciation goes to my supervisor, Mr. Lin Horng Sheng, for his sacrifices of time and energy to guide me in completing this report, despite major commitments to his family, doctorate, church, and other students. This project cannot be realized without his continual guidance and assistance. His emphasis on teaching a man to fish instead of giving him a fish will leave a great impact in my life.

In addition, I would like to thank my family and my family-in-law for the enormous mental and emotional support; my dear son, whose giggles and chuckles helped me go through every day; every single lecturer in UTAR who has dedicated their lives in teaching, especially those who taught Physics major. To quote an anonymous, "Teaching is not transmitting knowledge for students to learn what the teacher knows, it is moving others to enquire and learn what nobody knows yet."

Through this project, I am honoured to have met Jin Hao, who was my team mate for final year project competition; and Yusuf, who patiently taught me to use lab equipments and had been a good tutor.

Ultimately, I am thankful for the spiritual guidance provided by my Heavenly Father, whose presence is always with me. I can never thank Him more for the love He has showered over my life with all the help given to me during the making of this thesis.

REFRACTIVE INDEX CHARACTERIZATION OF FIBER SENSOR

ABSTRACT

This report aims to fabricate and to characterize the refractive index of a fiber sensor. The fiber sensor chosen for characterization is an in-line Mach-Zehnder interferometer (MZI). The sensor can be built by simply concatenating two abrupt tapers separated by a distance, L = 50 mm, using a splicing machine. The abrupt tapers featured a taper length, L_t = 700 μm and a taper diameter, D_t = 68 μm. Two refractive index (RI) range were tested: (i) 1.40-1.42; (ii) 1.40-1.50. Standardized Cargille oils were used as the RI solutions to immerse the tapers. The transmission spectra of the corresponding RIs were obtained by injecting broadband light source into the fiber. A wavelength shift and a change on the free spectral range indicate a change of RI. The fabricated sensor has achieved a maximum sensitivity of 146.3 nm/RIU (1.40-1.42) which is comparable to that of a long period fiber grating (LPFG) sensor. Compared to an LPFG sensor, MZI sensor promises ease of fabrication, cost effectiveness, robustness, and reproducibility. However, MZI sensor is only applicable for RI range 1.30-1.45.

The second RI range also included RI values above the fiber cladding RI, n_2 = 1.453, which is the limitation of MZI sensor. The MZI sensor transmission spectra obtained for $n > n_2$ were used to compare with the results obtained for a novel adiabatic taper fiber-based sensor, which was proposed at the end of this report. The proposed sensor has potentials in sensing high RIs of $n > n_2$ which can overcome the limitations of the sensing region for MZI sensor. The novel configuration will be suitable for future works to further implore the capability of fiber based sensors.

TABLE OF CONTENTS

LIST OF TABLES

LIST OF FIGURES

LIST OF SYMBOLS / ABBREVIATIONS

D_t	taper diameter
L	taper separation
L_t	taper length
n	refractive index
n_{eff}	effective refractive index
S	ratio of cladding to core diameter
z_t	local taper length-scale
Λ	grating period
λ	wavelength, m
λ_D	wavelength shift
$\Delta\lambda$	free spectral range
ρ	local core radius
ϕ	phase difference
BBS	broadband source
FBG	fiber Bragg grating
FSR	free spectral range
LPFG	long period fiber grating
MI	Michelson interferometer
MZI	Mach-Zehnder interferometer
OSA	optical spectrum analyzer
RI	refractive index
RIU	refractive index unit
SMF	single-mode fiber

CHAPTER 1

INTRODUCTION

1.1 Optical Fiber Sensor

Optical fiber is a transmission medium made of glass, used for transmitting light signals. It is, by far, the medium with the lowest attenuation (power loss). On top of that, because signals are in the form of light, data transfer speed is much better in an optical cable than in conventional copper wires.

Making use of the properties of an optical fiber and light, optical fiber can be used as a sensing device. Recently, optical fiber has been greatly employed in physical, chemical and biological sensing. This emerging trend is credited to some of its beneficial properties such as immunity to electromagnetic interference, lightweight, high availability and low signal loss that make optical fiber an excellent sensing instrument.

Fiber based sensor can be used to measure strain, displacement, temperature, pressure (Ghetia et al, 2013), current, and refractive index (RI) (Tian, 2009). Optical fibers are typically heated and stretched to a diameter compatible to the light source's wavelength, and the waist region is called a taper. In a taper, the fundamental core mode couples to the higher order cladding modes. These higher order cladding modes are sensitive to the surrounding's changes. By measuring the parameters which vary, an optical fiber based sensor can be characterized.

1.1.1 Light Propagation in an Optical Fiber

An optical fiber comprises of three parts: core, cladding and coating. The core's material is usually glass, and the cladding can be of glass or of plastic. The core refractive index, n_1 is higher than that of the cladding, n_2 so that light is confined within the core as it propagates along the waveguide. The refractive index difference between the core and the cladding is very small, the contrast, $\Delta = \frac{(n_1^2 - n_2^2)}{2n_1^2}$ is generally less than 1.

Light propagates through fiber due to total internal reflection. As Δ is very small, the maximum acceptance angle, α_{max} at which light must enter into the fiber in order for total internal reflection to occur, can be calculated using

$$\alpha_{\max} = \frac{\sin\left(n_1^2 - n_2^2\right)}{n_0} \qquad (1.1)$$

The total acceptance angle is then $2\alpha_{max}$, as seen in Figure 1.1.

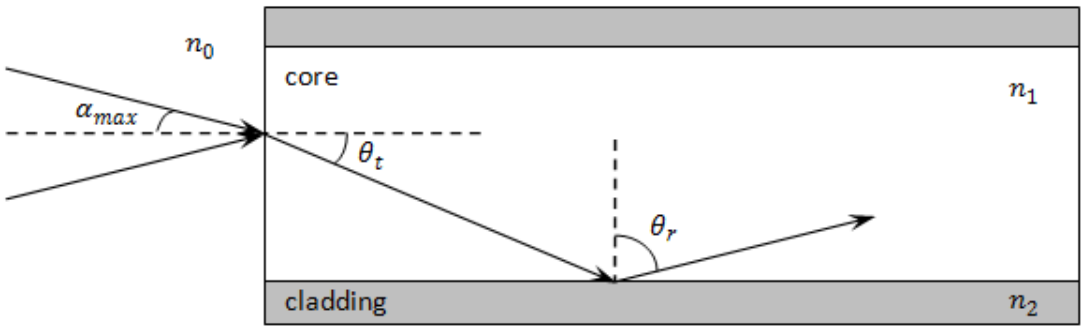

Figure 1.1: Acceptance Angle

Beyond $2\alpha_{max}$, any light which enters the fiber will be lost to the cladding as the reflected angle, θ_r exceeds the critical angle. The critical angle, θ_c is the minimum angle of θ_r required for light to experience total internal reflection. At any incidence

angle which exceeds the θ_c light will be reflected back into the glass medium (Fidanboylu et al, 2009).

Since$\Delta \ll 1$, light source is weakly guided along the optical fiber, meaning that some of the light will tend leak into the cladding. Higher modes have greater leakage as they penetrate deeper into the cladding. In a single-mode fiber (SMF), its core size is much smaller compared to the wavelength of light, therefore only the core mode can survive in the fiber. The V-number can be expressed in the following formula:

$$V = \frac{2\pi r}{\lambda}(n_1^2 - n_2^2)^{1/2} \qquad (1.2)$$

For V < 2.405, the fiber acts as an SMF. V changes with the core radius *r*, and light source wavelength λ.

1.1.2 Core-Cladding Transition

The core mode, LP_{01} is the only guided mode in a single-mode fiber. Its effective refractive index, n_{eff} lies between the core refractive index n_1 and the cladding refractive index n_2, $n_2 < n_{eff} < n_1$.

In a taper, however, the core and cladding diameters are reduced. This decreases n_{eff}. n_{eff} comes close to n_2 when the core diameter reduces in a taper. When $n_{eff} < n_2$, the fundamental core mode is no longer guided. It separates into modes that propagate in the cladding. According to Wang (2012), the core-cladding transition value is expressed as follows

$$V_{core/cladding} = \frac{2\pi}{\lambda}\frac{d}{2S}\sqrt{n_1^2 - n_2^2} \cong \sqrt{\frac{2}{\ln S}}\left(1 + \frac{0.26}{\ln S}\right)^{-1/2} \qquad (1.3)$$

where S is the ratio of cladding to core diameter. For SMF-28^{TM}, the core diameter is 8.2 µm, and the cladding diameter is 125 µm, which makes S = 15.24. Using the equation above, the calculated $V_{core/cladding}$ is 0.82. Theoretically, core-cladding transition takes place at a fiber diameter of 51.1 µm.

1.1.3 Adiabaticity of Taper

Ji et al (2013) have discussed that the taper length-scale must be much greater than the coupling length between the fundamental core mode and the cladding modes in an adiabatic taper, so that the power transfer from core to cladding transition is negligible (Wang, 2012). To achieve adiabaticity, the local taper angle, Ω(z) has to be small enough along the taper. Figure 1.2 shows $\tan\Omega(z) = \frac{d\rho(z)}{dz}$ (Love et al, 1991).

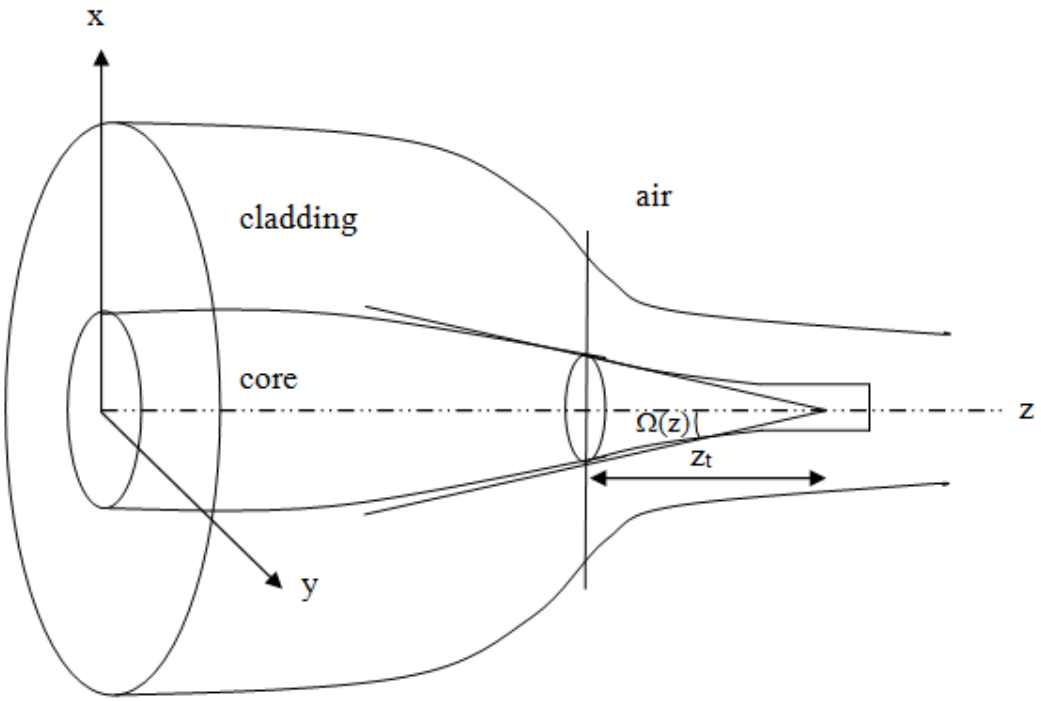

Figure 1.2: Down Taper of a Fiber with Finite Cladding

By using small angle approximation, the following is obtained

$$\Omega(z) \approx \frac{d\rho(z)}{dz} \approx \frac{\rho(z)}{z_t(z)} \qquad (1.4)$$

where

$\rho(z)$ = local core radius

$z_t(z)$ = local taper length-scale

The local coupling length, or beat length, z_b between the core mode and cladding modes is

$$z_b(z) = \frac{2\pi}{\beta_1(z) - \beta_2(z)} \qquad (1.5)$$

with $\beta = \frac{2\pi}{\lambda} n_{eff}$. When $z_t \gg z_b$, the adiabaticity criterion is fulfilled. When $z_t \ll z_b$, there is a great power transfer from the core mode to the cladding mode.

1.2 Problem Statement

The sensor reported in this thesis is an in-line Mach-Zehnder interferometer (MZI) sensor. It can be used for sensing RI of n < 1.453, which is the fiber cladding RI. The limitation of MZI sensor makes it unsuitable for testing liquids, mainly oils, of n > 1.453. Testing of oil RI can be applied for pollution sensing of the ocean from oil spills, and the reusability of cooking oils.

Oils of n < 1.453 can be detected by the MZI sensor, while a new sensor based on an adiabatic taper fiber is proposed at the end of this report to tackle the limitation of MZI sensor for testing of n > 1.453.

Fiber sensors are practical for oil sensing mainly due to their chemical resistance and the ability to withstand high temperature (especially for cooking oils with high smoking points). However, temperature characterization is required for sensing at a different ambient temperature than room temperature. The main focus of this report is solely on the refractive index characterization of an MZI sensor. A separate research on the combined effects of temperature and RI variations needs to be done for high temperature RI sensing.

1.3 Aims and Objectives

The report aims are:

- To fabricate an in-line Mach-Zehnder interferometer (MZI) sensor.
- To characterize the refractive index of the sensor.

This report will characterize the RI below that of the cladding, which is the limitation of an MZI sensor. For testing of oil, RI range of $n > 1.453$ needs to be detected as well, therefore a new sensor is proposed at the end of the report. It is however, not the main focus of this report, which will only investigate for RI $n < 1.453$.

The standardized RI liquids used for testing of MZI sensor are Cargille oils of RI range 1.40 to 1.50. The RI range involved for characterization were (i) 1.40-1.42 and (ii) 1.40-1.50. The second range involves $n > 1.453$ or the limitation of MZI sensor. The reason being the results obtained will be used for comparison with the new sensor proposed.

1.4 Thesis Outline

This thesis consists of five chapters with respective contents briefly described as follows.

- Chapter 1 provides a brief introduction of optical fiber sensor, total internal reflection and physics of taper.

- Chapter 2 presents a literature review on the recent development on different fiber based RI sensors.

- Chapter 3 includes the working principle of the fiber sensor and the methodology adapted to fabricate and characterize the sensor.

- Chapter 4 discusses on the results obtained from the experiment.

- Chapter 5 wraps up the thesis, making a conclusion and recommendations for further experimental works.

CHAPTER 2

LITERATURE REVIEW

In this chapter, a review on different sensor types and their recent developments is done. In Section 2.4, two comparison tables are listed to compare and contrast the advantages and limitations between the sensor types.

2.1 Long Period Fiber Grating (LPFG)

Long period gratings are gratings inscribed periodically on fiber to introduce refractive index modulation. Figure 2.1 shows a schematic diagram for a typical LPFG configuration.

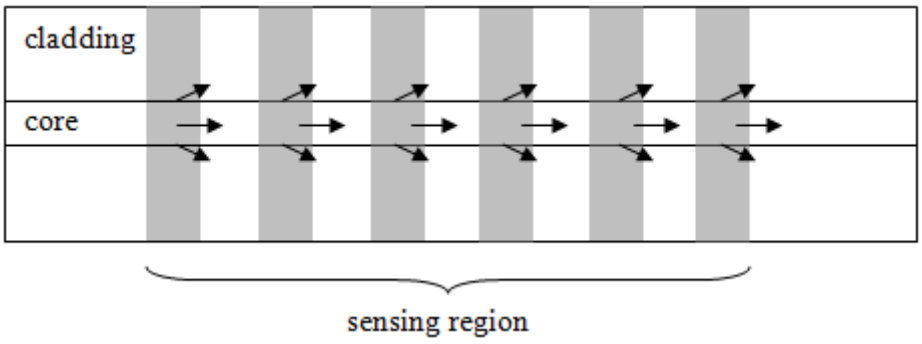

Figure 2.1: LPFG Configuration

The phase matched condition reported by Kheiri et al (2011) for LPFG is expressed by the resonance wavelength,

$$\lambda_m = \left(n_{co}^{eff} - n_{cl,m}^{eff}\right)\Lambda = \partial n_{eff}\,\Lambda \qquad (2.1)$$

where

n_{co}^{eff} = effective RI of core mode at λ_m

$n_{cl,m}^{eff}$ = effective RI of m-th cladding mode at λ_m

Λ = grating period

The RI sensitivity depends on the resonance wavelength.

LPFG can be fabricated using ultraviolet (UV) laser, CO_2 laser, etching, carving (Zhu et al, 2007), ion implantation, femtosecond infrared laser, or arcing (Kheiri et al, 2011). The etching and carving methods are destructive to the optical fiber as they will produce periodic grooves on the fiber cladding. Such fabrication methods will weaken the fiber mechanical structure, introduce contamination and increases the polarization-dependent loss (PDL).

Zhu et al (2007) reported a novel, non-destructive LPFG structure by making use of the thermal shock and fast cooling effects of the CO_2 laser which introduces refractive index disturbance on the cladding edge. It was found that such structure not only reduces the PDL, its sensitivity also exceeds that of the conventional LPFG. In the RI range of 1.33 to 1.45, its maximum wavelength shift was 24.2 nm. In more recent paper, Zhu et al (2009) again demonstrated the potential of edge-written LPFG in refractive index sensing which was able to achieve 741 nm/RIU in the range of 1.43 to 1.45.

A cost-effective and versatile LPFG sensor was proposed by Kheiri et al (2011) fabricated using electrical arc discharge to increase the fiber diameter. The grating length was 8 mm, with periodic fattened fiber sections separated by a distance of 0.5

mm. For an RI range of 1.315 to 1.3618, a maximum sensitivity of 134.18 nm/RIU was obtained.

To further improve its sensitivity, Ji et al (2013) have reported an RI sensor by inscribing LPFG on an adiabatically tapered fiber. The photosensitive fiber has double claddings, in which the inner cladding was doped with boron and germanium. The maximum sensitivity achieved was around 600 nm/RIU for RI 1.3461 to 1.3791. Despite the fiber was tapered beforehand, the gradual decrease in diameter ensures a better mechanical strength of the fiber sensor.

A combination of LPFG with Michelson and Mach-Zehnder interferometer can be done to increase its sensitivity in RI sensing as demonstrated by Shi et al (2011). This report will further implore the combination of LPFG and MZI in the later section.

Despite its high sensitivity, LPFG has its own drawbacks. Aside from a weakened mechanical strength, it requires precise and expensive masks. In order to reduce PDL, multiple exposure fabrication method has to be used, which further increases the complexity of fabrication.

2.2 Fiber Bragg Grating (FBG)

The FBG is similar to LPFG as it is also consists of periodic RI modulations on a fiber. According to Tian (2008), the difference is that the period is usually on the order of hundreds of nanometers.

The gratings act as a mirror for light in a range of wavelength, which can be obtained by

$$\lambda = 2n_{eff}\Lambda \qquad (2.2)$$

where n_{eff} is the effective RI of core mode, Λ is the grating period. Light of other wavelengths will not be affected by the Bragg grating. The range of reflected light wavelength is very narrow, with a typical bandwidth of below 1 nm. Bragg reflection is illustrated in the following figure.

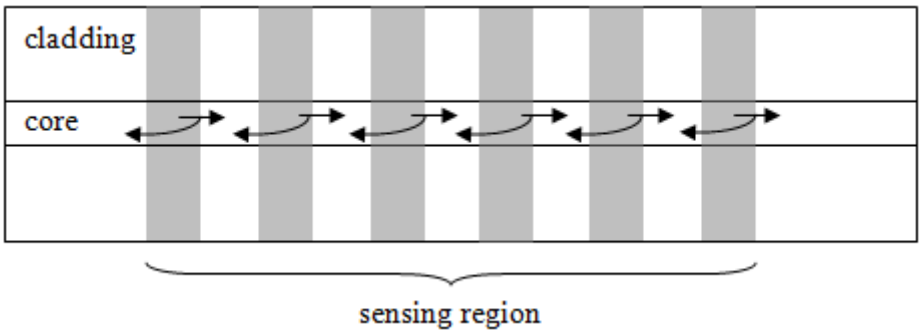

Figure 2.2: FBG Configuration

FBG promises a high resolution up to 4×10^{-5} (Iadicicco et al, 2005), and Gouveia et al (2012) reported a sensitivity of 106 nm/RIU for their Fabry-Pérot cavity based on FBG sensor.

Based on theoretical calculations, Liang et al (2011) was able to simulate an FBG based refractometer in macro/nanofiber with a high sensitivity of 993 nm/RIU.

By etching the fiber core, the resolution and sensitivity are greatly increased, achieving up to 1394 nm/RIU with a minimum resolution of 7.2×10^{-6} as shown by Chryssis et al (2005) but the trade off was a huge reduction in the sensor's mechanical strength and durability.

2.3 Interferometric Sensors

Interferometry based sensor splits the optical signals into two separate arms: the sensing arm and the reference arm. In this section, discussion on MZI and Michelson interferometer (MI) sensors is made.

2.3.1 Mach-Zehnder Interferometric Sensor

Interferometric sensors can be achieved two ways: duo-arm or in-line. In-line interferometry confines the arms into one single fiber: using the core mode and the cladding modes as the "arms". MZI sensors can be further enhanced using LPFG, FBG or core/cladding mismatch. In this section, some of the MZI configurations done recently is discussed. A comparison table between these MZI configurations is listed in Section 2.4 to justify this report's focus on in-line taper based MZI.

2.3.1.1 In-Line Taper Based MZI

An in-line Mach-Zehnder interferometer (MZI) is basically an optical fiber with two concatenating abrupt tapers. This is illustrated in Figure 2.1.

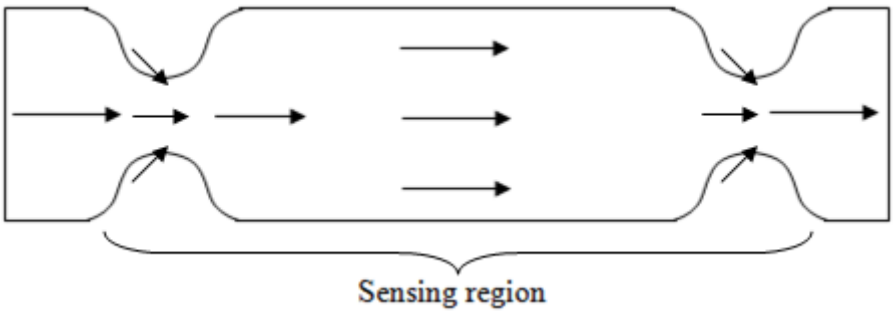

Figure 2.3: In-line Mach-Zehnder Interferometer

Figure 2.3 illustrates two fiber tapers separated by a distance, which is essentially the sensing region of the interferometer. In the first taper, the core mode that travels through the fiber couples into higher-order cladding modes, leaving part of the energy to propagate within the core. These cladding modes in the evanescent field are highly sensitive to the surrounding refractive index changes (Chen et al, 2013). In the second taper, the cladding modes couple back to the core mode.

A simple, in-line MZI sensor was demonstrated by Tian (2009) by constructing a pair of 3 dB tapers. He has achieved a maximum sensitivity of 17.1 nm/RIU for RI 1.315 to 1.3618.

2.3.1.2 Duo-Arm MZI

An improved, duo-arm MZI sensor was reported by Yu et al (2014). Two polytrimethyleneterephthalate (PTT) nanofibers were used as the sensing and reference arms. One of the fiber segments was bent with an S-shape above the other fiber segment. The two segments were drawn close to each other to form the sensing region. The sensitivity achieved using this new structure was 1100 nm/RIU for RI 1.34 to 1.39.

According to Tian (2009), a two-arm fiber sensor is complicated to fabricate because the reference signal needs to be stabilized.

2.3.1.3 LPFG Based MZI

To further enhance the performance of a sensor, modal interferometry can be realized using LPFG. Such sensor is fabricated by placing two identical LPFGs in series with a cavity length in between to form an interferometer. The LPFG pair is immersed in the measurand and the spectral shift is observed according to different RI (Silva et al, 2012).

Its potential was explored as early as 1996 by Dianov et al, which promises low temperature sensitivity, capability with the use of a low-coherent source and ease of fabrication. The sensor proposed was capable of sensing RI in the range of 1.4 to 1.45 with a minimum resolution of 10^{-3}. For liquid of RI larger than the cladding RI, the interferometer was able to tell the presence of the liquid by monitoring the transmission spectrum.

Ding et al (2005) have realized a LPFG pair based MZI to be used in RI sensing. They have added a fiber taper section of length 16 mm in between the LPFG pair to enhance the sensitivity. The resulting sensitivity was 173.8 nm/RIU. It was found that increasing the taper length improves the sensitivity achieved.

In the paper prepared by Fu et al (2011) has demonstrated the different characteristics in response to varying the cavity length between the grating pair. Different spacing between the gratings would affect the detectable RI range. At 80 mm the sensor was sensitive to RI 1.431 to 1.45, being highly sensitive to 1.45 with the least sensitivity to 1.431. At 250 mm the sensor was used for RI 1.33 to 1.413, being highly sensitive to 1.413 yet the least sensitive to 1.33. The potential of the sensor in measuring the liquid level was reported.

2.3.1.4 MZI Based FBG

Since FBG in SMF is usually insensitive to the external RI, Liao et al (2010) has demonstrated a sensor which has two cavities that form an interferometer within an FBG. The two cavities are essentially sections with the core near to the core-cladding interface removed. In the first cavity, light split into core mode and cladding modes, which recombine at the second cavity. The phase difference induced by the external RI change is observed and a sensitivity of 9148 nm/RIU is obtained for RI 1.30 to 1.325.

2.3.1.5 Core/Cladding Mismatched MZI

A core mismatch based MZI was reported by Shi et al (2011) by splicing a thin-core fiber (TCF) between two SMFs. The TCF has a core diameter of 4.8 μm, about half the core diameter of SMF. The core mismatching leads to the core mode coupling to cladding modes at the SMF-TCF interface, which would then couple back to core mode at the TCF-SMF interface. The sensitivity was reported to be 44.7 nm/RIU for RI 1.333-1.375.

The second configuration presented in this section was fabricated by Pang et al (2011). Two double cladding fibers (DCFs) were made to cascade in an SMF. In the first DCF, the fundamental core mode partially splits into the cladding modes. The cladding modes propagate along the outer cladding of DCF, while the remaining light continues to propagate along the core. These modes travel along the SMF that is sandwiched between the DCFs. Then, they recombine in the second DCF. By dipping the whole DCF-SMF-DCF structure into the measurand, a maximum sensitivity of 31nm/RIU was obtained for RI=1.33, and 823 nm/RIU for RI=1.44.

2.3.2 Michelson Interterometric Sensor

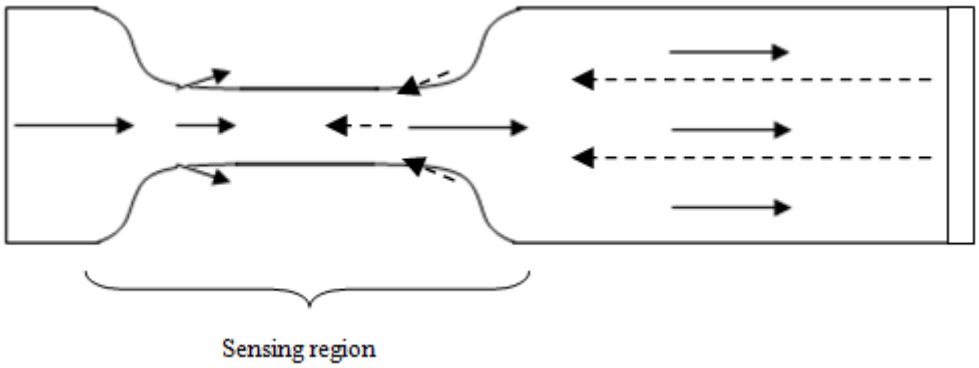

Figure 2.4: In-line Michelson Interferometer

A Michelson interferometer is similar to Mach-Zehnder interferometer. In a Michelson interferometer, light that propagates along the fiber will go through the same taper twice. The first time it goes through the taper, light signals split into core mode and cladding modes. At the fiber end, light will be reflected back by a mirror deposited on the fiber tip and travel through the taper once more, where cladding modes interfere with the remaining core mode. The mirrors can be formed by depositing dielectric or metal coatings on the fiber tips (Kashyap, 1983).

A rectangular cavity was drilled into the fiber's core-cladding interface by using laser pulses, and then the section of fiber was cleaved to reveal the rectangular groove. A thin film of silver was coated on the revealed core surface and the fiber end as a mirror. This in-line Michelson interferometer sensor demonstrated by Liao (2012) has achieved a maximum sensitivity of 975 nm/RIU.

2.4 Summary

Table 2.1: MZI Sensor Types

MZI type	Sensitivity	Advantage	Limitations
In-line Taper	17.1 nm/RIU	• Compact • Ease of fabrication • Cost effective	• Low sensitivity
Duo-arm	1100 nm/RIU	• High sensitivity	• Difficulty of fabrication
LPFG	173.8 nm/RIU	• Can be used to measure liquid level	• Complexity of fabrication • Expensive • Requires more measurand
FBG	9148 nm/RIU	• Extremely high sensitivity • High resolution	• Complexity of fabrication • Expensive • Small sensing range
Core/Cladding Mismatch	823 nm/RIU	• High sensitivity for high RI	• Needs special fiber • Complexity of fabrication • Small sensing range

Table 2.2: All RI Sensor Types

Sensor Type	Sensitivity	Advantage	Limitations
LPFG	741 nm/RIU	• High sensitivity • Big RI range	• Complexity of fabrication • Expensive • Fragile
FBG	1394 nm/RIU	• High resolution • Multiplexing capability	• Special configurations needed for RI sensing • Low sensitivity (high sensitivity in exchange for fragility and low durability)
MZI	9148 nm/RIU	• High sensitivity • Compact • Ease of fabrication	• Duo-arm MZI more difficult to fabricate
MI	975 nm/RIU	• High sensitivity • Compact	• Need for high precision during fabrication • Large PDL

2.5 Thesis Contribution

In this thesis, an in-line MZI sensor is proposed. The sensor type was chosen for advantages such as:

- Simplicity
- Cheap
- Robustness
- Ease of fabrication
- Moderate sensitivity
- High reproducibility

An in-line MZI can be constructed in less than two hours for an experienced student. The author took almost three hours in making the first in-line MZI sensor. Although the literature review above showed that an in-line MZI sensor may not have a high sensitivity, such configuration is sensible to be done as a final year project as the same sensor can be re-fabricated anytime with a simple setup. Besides, comparing it to a basic LPFG sensor of the highest sensitivity at 173.8 nm/RIU, MZI promises robustness and cost effectiveness.

CHAPTER 3

METHODOLOGY

3.1 Working Principle

We have chosen the MZI configuration from the list of the sensor types made in Chapter 2 due to its compactness, ease of fabrication, mechanical strength and economic advantages.

As discussed in earlier chapters, the operation of in-line MZI is based on confining the sensing and the reference arms in the cladding and the core. In the first taper, the fundamental core mode LP_{01} is excited to higher order cladding modes LP_{nm}. The excited cladding modes propagate outside the core i.e. along the cladding, and the remaining light energy continues to propagate along the core as the core mode, and a phase difference between the cladding and core modes is introduced. The phase difference is expressed as follows:

$$\phi = \frac{2\pi \Delta n_{eff} L}{\lambda} \qquad (3.1)$$

where

Δn_{eff} = effective RI difference between the core and cladding modes, RIU

L = interference length or the separation distance between the two tapers, m

λ = wavelength the light injected, m

On the other hand, the light energy remaining in the core mode is given by

$$I = \left(\sum_{i=1}^{10} a_i^0 \cos \Delta\varphi_{0i} \right)^2 + \left(\sum_{i=1}^{10} a_i^0 \sin \Delta\varphi_{0i} \right)^2 \qquad (3.2)$$

The cladding modes will interfere with the core mode in the second taper. When $\phi = (2n + 1)\pi$ which is odd times of π, the interference signal reaches a dip in transmission, and equation (3.1) becomes

$$\lambda_D = \frac{2\Delta n_{eff} L}{2n+1} \qquad (3.3)$$

where

λ_D = transmission dip wavelength, m

n = integer

The interference will be affected by the external RI, in this case, the measurand RI, and a wavelength shift occurs in the transmission spectrum. When a measurand is applied onto the taper, effective RI of cladding or n_{eff} increases by δn_{eff}, and Δn_{eff} decreases by δn_{eff} since n_{eff} value becomes closer to the value of effective RI of core mode. Due to a decrease in Δn_{eff}, according to equation (3.3) λ_D will therefore shift to a shorter wavelength.

Aside from the wavelength shift, the free spectral range (FSR), which is the spacing in wavelength between two successive intensity maxima/minima, will also change with the surrounding RI, according to the equation

$$\Delta\lambda = \frac{\lambda^2}{\Delta n_{eff} L} \qquad (3.4)$$

which means a decrease in Δn_{eff} will shift the FSR to the longer wavelength. To characterize the RI sensor, the wavelength shift and FSR in response to the external RI change were used.

3.2 Fabrication

An SMF-28^{TM} optical fiber is used for the fabrication of the MZI sensor in this report. The core diameter of a typical SMF-28^{TM} is 8.2 μm and cladding diameter is 125 μm, with core RI, $n_1 = 1.458$ and cladding RI, $n_2 = 1.453$. Both ends of the fiber were each spliced to a pigtail using a fusion splicer. A section of the fiber is stripped to remove the coating and the fiber was cleaned using ethanol solution to remove debris.

Tapers can be fabricated using a number of methods, namely electrical arc discharge, flame brushing and chemical etching (Wang, 2012). In this thesis report, we have employed the electrical arc discharge method to fabricate the first type of sensor by simply cascading two abrupt tapers. The tapers were fabricated with an Ericsson fusion splicer's built-in tapering program and assumed to be identical. Figure 3.1 depicts one of the tapers fabricated using the fusion splicer.

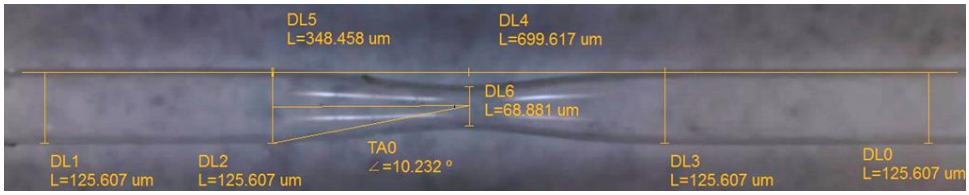

Figure 3.1: Taper As Viewed Under a Microscope.

The fabrication of the sensor was easy and precise without the need of special fabrication skills, and the sensor can be easily replicated in any laboratory equipped with a fusion splicer. The fabrication was not time-consuming. For a skilled student, the sensor can be constructed less than one hour.

3.3 Setup and Procedure

The fiber was connected to the broadband source (BBS) and to the optical spectrum analyzer (OSA) using the pigtails. The BBS injects light signals into the fiber and observation on the corresponding transmission spectrum was studied on a computer via the OSA. Wavelength range used was 1450 nm to 1560 nm. Figure 3.2 and 3.3 illustrate the experiment setup.

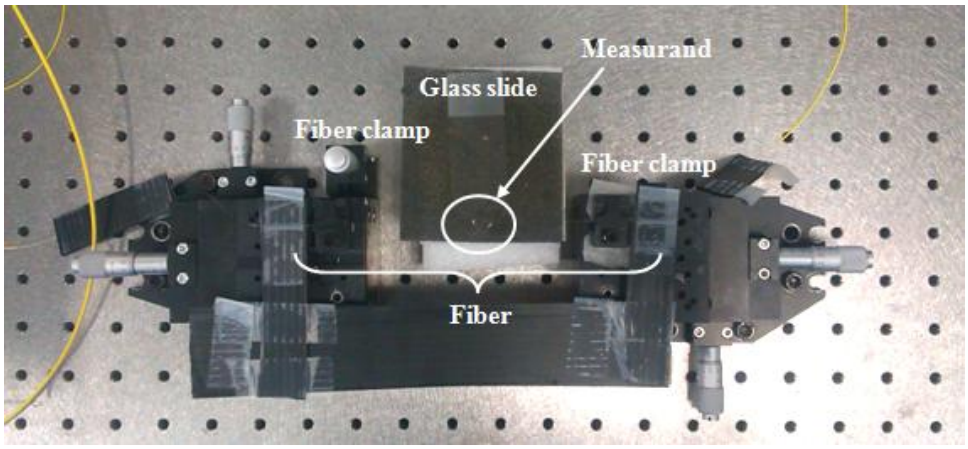

Figure 3.2: Experiment Setup for RI Sensing.

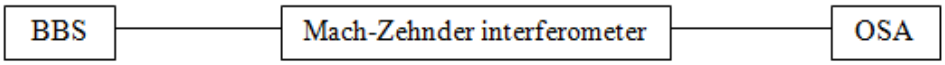

Figure 3.3: Schematic Diagram of Experiment Setup.

The fiber was mounted on a fixed stage and both ends of the fiber were held in place with fiber clamps to ensure no macroscopic bending. A stage was placed underneath the fiber with a microscope glass slide. Measurands used were Cargille oil solutions of standardized RIs.

In the experiment, the standardized RI liquid was dropped onto the slide and the sensing regions as shown in Figure 3.4 (a) was dipped in the liquid by adjusting the stage and immersing the fiber into the solution.

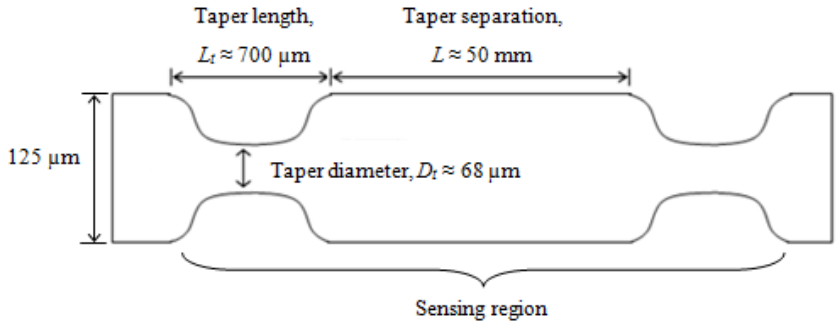

Figure 3.4: Sensing Region of MZI Sensor.

After recording the output spectrum for the first RI, the fiber and the stage were cleaned with an alcohol solution to obtain the reference spectrum. Then, a new RI solution was applied and its corresponding output spectrum was recorded. The same procedure of cleaning and applying was repeated until all RI solutions were tested.

CHAPTER 4

RESULTS AND DISCUSSION

The results obtained for the MZI sensor are discussed in this chapter. Two RI range used to test the sensor: (i) 1.40-1.42; (ii) 1.40-1.50.

4.1 Mach-Zehnder Interferometric Sensor

To characterize the Mach-Zehnder interferometric sensor, light from the BBS was injected into the fiber and the spectral response was recorded by the OSA for the wavelength range of 1450 nm to 1560 nm. The reference spectrum recorded is shown in Figure 4.1.

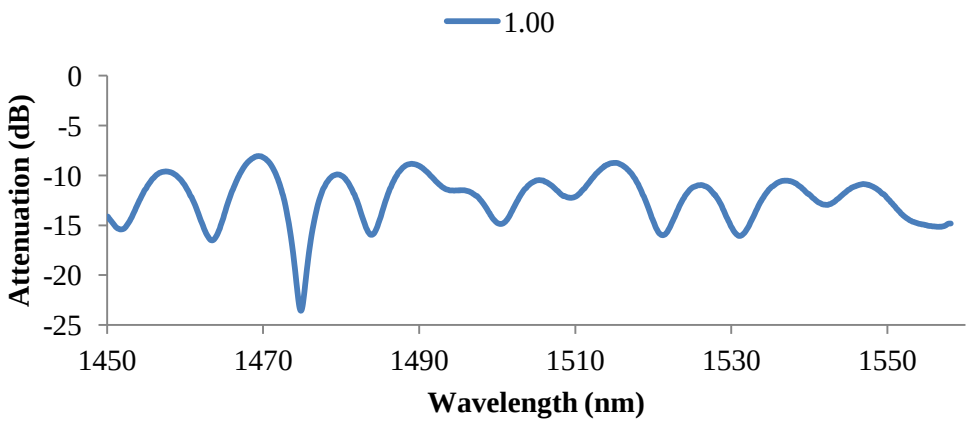

Figure 4.1: Reference Spectrum of the MZI Sensor.

Two sets of data were obtained for MZI sensor using two different RI range. Both sets provided a good linear response, each with sensitivity above 1.00 nm for a 1% RI change.

The first set was done using RI: 1.4000, 1.4040, 1.4080, 1.4120, 1.4160 and 1.4200; the second set was done using RI: 1.40, 1.42, 1.44, 1.46, 1.48 and 1.50. For the second set, the first three solutions have RIs below cladding RI, n_2 while the last three have RIs exceedingn_2.

For the experiment, the tapers of MZI sensor were dipped in each of the liquid and the corresponding output spectra were recorded. The results for the first set (RI 1.40 to 1.42) and the second set (RI 1.40 to 1.44) were analysed in Figure 4.2. Both sets provide a good linear response, with sensitivity each of 1.46 nm and 1.24 nm for a 1% change in RI.

4.2 Characterization of Sensor

4.2.1 Wavelength Shift

From the equation (3.3) that was mentioned in Chapter 3, a wavelength shift occurs when Δn_{eff} changes byδn_{eff}. This change was induced during the experiment, when an RI liquid was applied onto the fiber tapers and they become the cladding due to the downsizing of taper. Δn_{eff} is the difference in the effective RI between the core and the cladding. The core RI is always large than the cladding RI, in order for effective light confinement within the fiber.

In the taper, since the core has disappeared, the cladding essentially replaces the core, while the RI liquid becomes the cladding. Therefore, Δn_{eff} becomes the difference in the effective RI between the cladding (which is now the core) and the liquid RI (which is now the cladding). Such wavelength shift can be observed in the figure that follows.

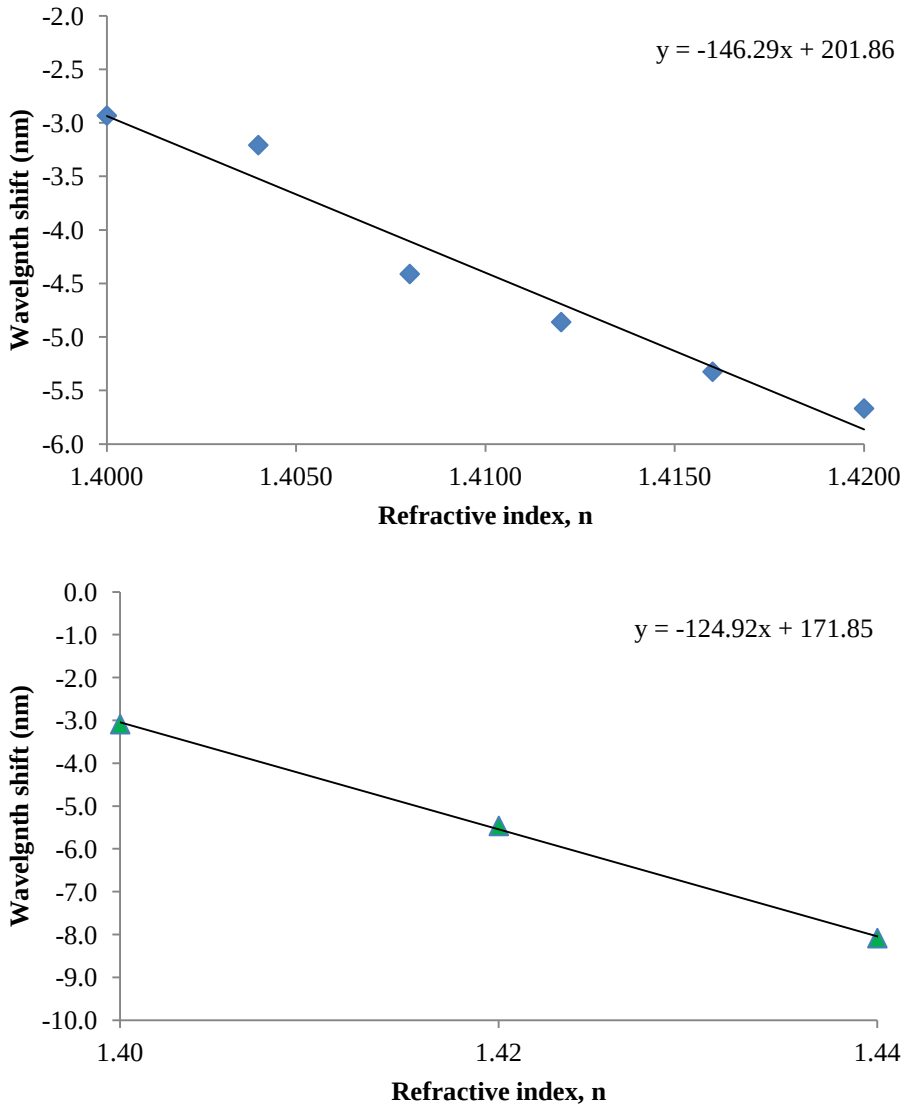

Figure 4.2: Wavelength Shift: (a) First Set RI 1.40-1.42 (Left); (b) Second Set RI 1.40-1.44 (Right).

According to equation 3.3, a wavelength shift occurs when n_{eff} changes byδn_{eff}. As the surrounding RI increases from 1.40 to 1.44, the difference between effective core RI and effective cladding RI, Δn_{eff} decreases by δn_{eff}, since core RI is higher. Equation (3.3) predicted a shift to a shorter wavelength when surrounding RI increases. This is evident in Figure 4.2.

Results for RI 1.46 to 1.50 were not plotted in Figure 4.2 (b) but their transmission spectra are shown in Figure A.3 in the appendix. Since these RI values

were aboven_2, thus they cannot be sensed by the MZI sensor as there will be no interference between the core mode and the cladding modes, because most of the cladding modes will be lost to the surrounding, which is the RI sample.

For the first set of values, a good linear response was obtained for RI 1.40 to 1.42. Six samples were used, with a gap of 0.004 RIU. The sensitivity achieved was 146.3 nm/RIU, which was rather satisfying for a sensor with such a simple configuration.

According to Table 2.1, such sensitivity was comparable to that of MZI-LPFG sensor with a sensitivity of 173.8 nm/RIU, which requires a more sophisticated fabrication and decreases the sensor's robustness.

For the second set of values, a good linear response was also obtained for RI 1.40 to 1.44. Only three data were plotted in Figure 4.2 (b), since RI 1.46 to 1.50 did not show interference in their respective transmission spectra. The sensitivity achieved was 124.9 nm/RIU.

The percentage difference of the wavelength shift per RIU achieved by the first set and the second set of data is as shown by the calculation that follows.

$$\text{Percentage difference} = \frac{|146.3 - 124.9|\ nm/RIU}{146.3} \times 100\% = 14.6\%$$

The difference of 14.6% may be contributed by the larger gap between the successive RIs of the second set (a gap of 0.02 RIU) compared to the smaller gap between the successive RIs of the first set (a gap of 0.004 RIU).

Besides, the first set of RIs corresponded to a narrower range than that of the second set. Different RI range can produce varying sensitivities. This was demonstrated in a research by Pang *et al.* (2011), in which they have fabricated an in-line MZI sensor based on double cladding fibers. A sensitivity of 31 nm/RIU was

achieved for the lower RI (1.34), while a sensitivity of 823 nm/RIU was obtained by the higher RI (1.44).

4.2.2 Extinction Ratio

The transition of the power spectrum was evident in terms of the extinction ratio. The extinction ratio is the height difference between a maximum and its successive minima, or vice versa. From RI 1.40 to 1.44, the maximum extinction ratios are larger than 3 dB. At RI = 1.46, the maximum extinction ratio immediately dropped to about 1 dB. This was the case for RI 1.48 and 1.50.

The drop in the extinction ratio for $n > n_2$ suggests a lack of interference between the core mode and the cladding modes. The results based on extinction ratio are analysed in Figure 4.3. The figure shows the maximum extinction ratio for $n > n_2$ was no more than 3 dB which contrasted greatly to the spectral responses demonstrated by RI $n < n_2$. The transmission spectra can be observed from Figure A.2 and Figure A.3.

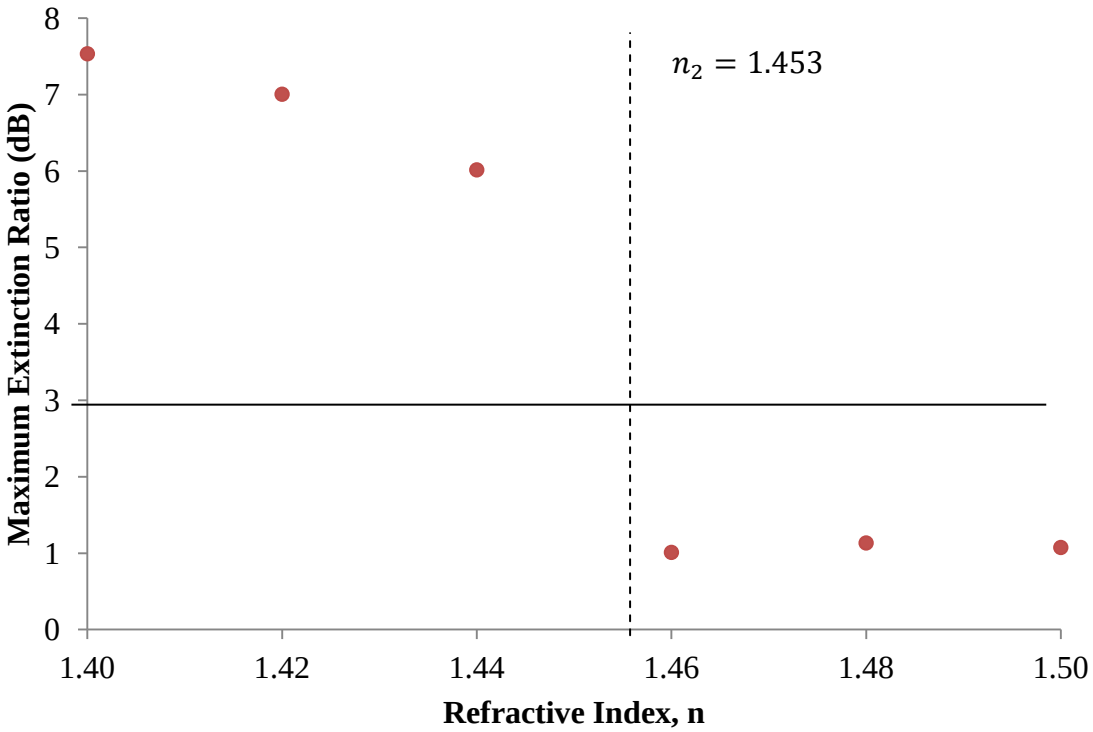

Figure 4.3: Maximum Extinction Ratio of RI 1.40 to 1.50.

4.2.3 Free Spectral Range

From the equation (3.4) shown in the previous chapter, it is known that $\Delta\lambda$ or the FSR increases with a decreasing Δn_{eff}. Δn_{eff} changes by δn_{eff} when the surrounding of the tapers are applied with RI liquid. In the experiment, the sample RI was increased from

a) 1.40 to 1.42 for the first set of procedures, and
b) 1.40 to 1.50 for the second set of procedures.

Therefore, the liquid RI becomes closer to the value of the cladding RI (which is the core of the taper), which decreases the value of Δn_{eff} by δn_{eff}.

In Figure 4.4, the experimental FSR for different RIs of both sets are plotted. There exists an outlier in Figure 4.4 (a) for the case of RI 1.40 to 1.42. The sensitivity of this range is much higher than 1.40-1.50. From the data fitted line, the first set of values shows a steeper gradient at 80 nm/RIU, while the second set demonstrates a rather flat gradient at ~ 6 nm/RIU.

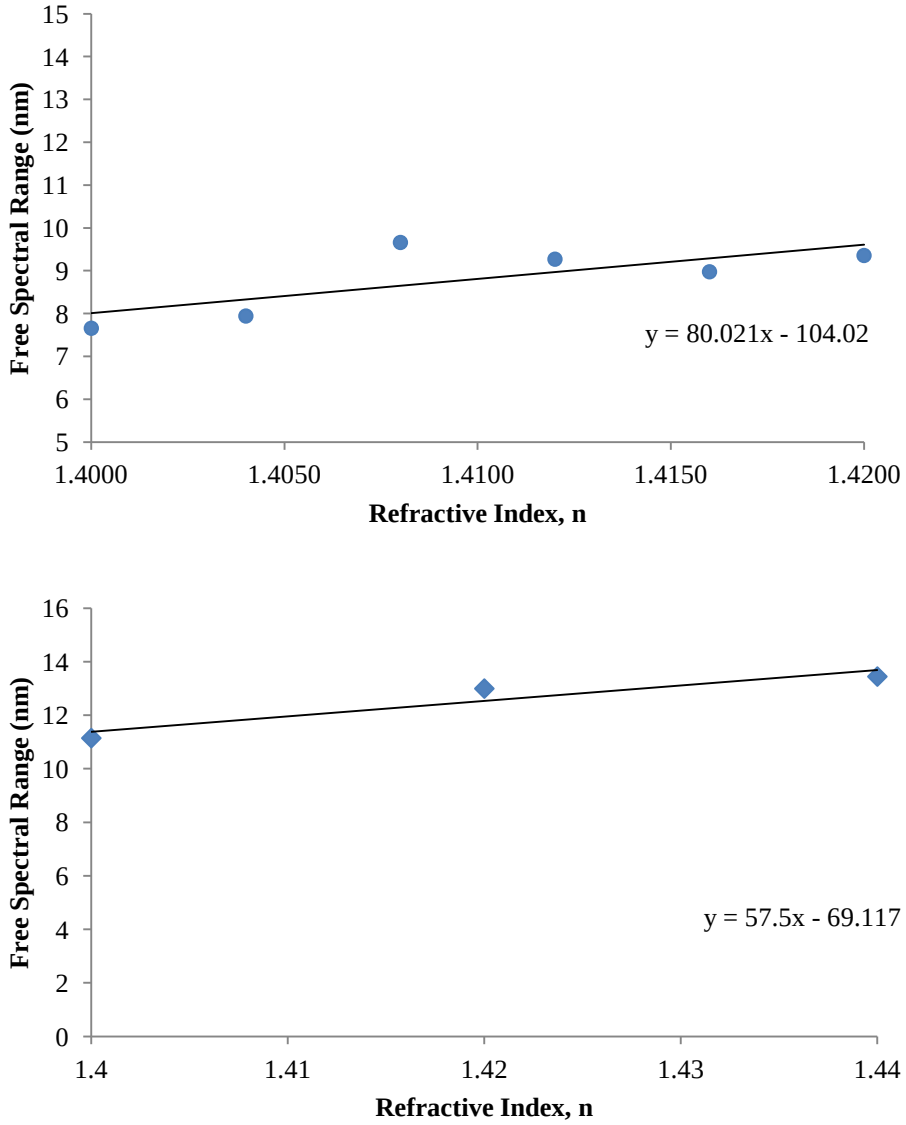

Figure 4.4: FSR: (a) First Set RI 1.40-1.42 (Left); (b) Second Set RI 1.40-1.44 (Right).

The percentage difference between the sensitivities achieved using FSR is

$$\text{Percentage difference} = \frac{|80.0 - 57.5|\, nm/RIU}{80.0} \times 100\% = 28.1\%$$

The difference in sensitivities achieved by both sets may be due to the different range of wavelengths used to determine the FSR. For analysis purpose, wavelength regions with high extinction ratios are used in order to ensure maximal interference between the core mode and the cladding modes. For the first set of data, the wavelength region used for analysis is between 1470 nm to 1485 nm. For the second set of data, the wavelength region used is between 1515 nm to 1535 nm. The FSR equation (3.4) shows that the wavelength of the light source will definitely affect the FSR value. From the same graph, many sets of FSR can be calculated as there are at least eight maxima or minima pairs. Hence, various FSR values can be attained for a single plot.

Besides, for the second set, only three RI values are used for analysis purpose, as values 1.46, 1.48 and 1.50 exceed the cladding RI and no interference pattern can be analysed. It is believed that, if more RI values were used, a better sensitivity of the sensor can be achieved in terms of FSR.

Comparing the percentage differences obtained for wavelength shift in subsection 4.1.2 which is 14.6% and FSR in this subsection which is 28.1%, the author believes that characterization in terms of wavelength shift would be more suitable due to a higher consistency, as the same method was employed in various papers such as by Tian (2009), Shi *et al.* (2011) and Pang *et al.* (2011).

CHAPTER 5

CONCLUSION AND RECOMMENDATIONS

5.1 Conclusion

An in-line Mach-Zehnder interferometric sensor was successfully fabricated and characterized in this report. The fabrication of the interferometer was relatively easy and less time consuming, compared to other fiber based sensors. The sensor was created by concatenating a pair of 3 dB abrupt tapers separated by a distance of 50 mm on a single-mode fiber using a fusion splicer. The reported configuration has a high reproducibility, therefore similar results can be achieved by other experimenters using the same setup.

From the experimental results, the maximum wavelength shift per refractive index unit is measured to be 146.3 nm/RIU, while the maximum free spectral range is measured to be 80.0 nm/RIU, for RI 1.40-1.42. The maximum sensitivity of the sensor is therefore 146.3 nm/RIU.

Although in the second set (1.40-1.44) the refractive index range used was supposedly 1.40-1.50, values above 1.44 were not considered for characterization since the sensor was incapable of sensing refractive index higher than that of its cladding ($n_2 = 1.453$). The responses for RI 1.46-1.50 were obtained for the purpose of comparison between the proposed sensor and the novel sensor configuration that is described in the following paragraph.

A novel fiber based sensor was proposed in this thesis in the following subsection. The novel sensor has promising sensing capability for refractive index higher than that of the cladding, which was a limitation of the reported Mach-Zehnder interferometric sensor.

5.2 Future Works

5.2.1 MZI Sensor with Adiabatic Taper

As demonstrated by Tian (2008) and Ding et al (2005), an adiabatic taper may enhance the sensitivity of an MZI or an LPG sensor by a factor of 2 to 4. Tian (2008) has reported an enhanced sensitivity of 3.4 times for a similar configuration, using a 62 mm MZI with an 11 mm long slow taper of waist 40 μm fabricated afterwards. The sensitivity achieved was 0.77 nm per 1% RI change or 77 nm/RIU.

In this paper, the same approach was also done on an MZI sensor. An attempt of fabricating a similar configuration by creating a gentle taper after fabricating the abrupt taper pair was done, but to no avail. The abrupt tapers had increased the vulnerability of the fiber to breaking. When the fiber was clamped on the stages for flame brushing, the fiber broke due to downsizing of the fiber diameter at the abrupt tapers.

Therefore, the fabrication steps were reversed. A section of 20 mm was flame brushed and stretched to a waist diameter of 35 μm. Before fabricating the abrupt taper pair, the adiabatically tapered fiber had been subjected RI testing in order to check for RI changes. After going through the same set of procedures by applying RIs and observing the respective transmission spectra, the fiber was cleaned and an abrupt taper was fabricated on either side of the adiabatic taper.

In contrast to an enhanced sensitivity that was anticipated, for RIs 1.40, 1.42 and 1.44, the spectral responses showed no interference between the fundamental core

mode and the cladding modes. The result is as shown in the Figure A.4 in the appendix.

For RIs above cladding RI, which were 1.46, 1.48 and 1.50, drastic changes occurred. For $n = 1.46$, which was the closest RI value used in this experiment to n_2 = 1.453, demonstrated the largest attenuation in optical power, by achieving a power loss between 60 to 70 dB. For n = 1.48, the power line shifted higher up, to above -40 dB. For n = 1.50, the power line shifted even higher than 1.48, to -30 dB. Similar trend was obtained for the adiabatic taper fiber that was tested without the abrupt taper pair. With the results obtained for this configuration, it was decided that a new sensor was to be proposed. This will be discussed in the next subsection.

5.2.2 Adiabatic Taper Fiber Sensor

The adiabatic fiber sensor featured in this subsection had a length of 50 mm with a waist of 40 μm. The spectral responses demonstrated were similar to that of the results in the aforementioned subsection. For RI of n = 1.40, 1.42 and 1.44, the attenuation lines maintain around -3 dB with no interference taking place. When RI 1.46 solution was applied on the fiber, the attenuation line dropped to the lowest, at -30 dB and below. Then, attenuation line shifted up for 1.48, and even higher for 1.50. The attenuation shift can be observed in Figure 4.5.

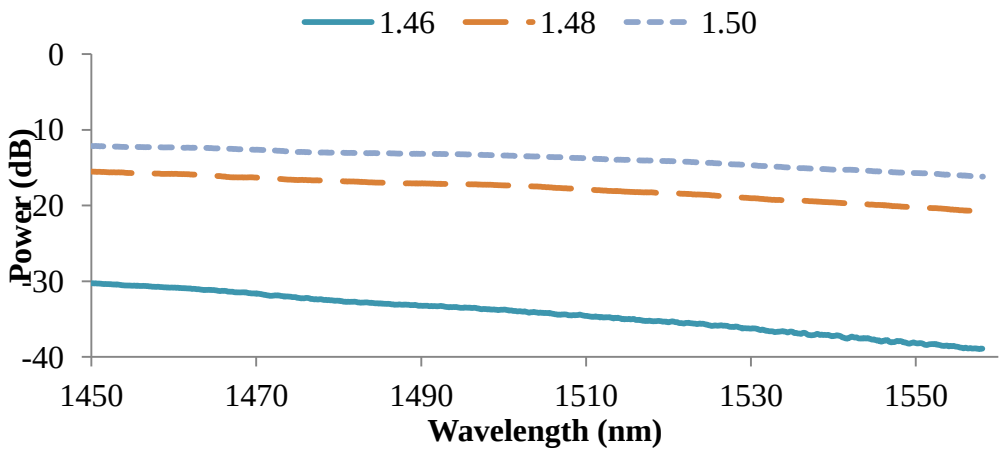

Figure 5.1: Spectral Response for $n > n_2$.

5.3 Recommendations for Sensing $n > n_2$

In this report, refractive index sensing using a sensor comprising of a gentle taper was attempted, as recommended in the thesis written by Tian (2008). A fiber sensor based on a gentle taper with a taper length of 50 mm and a taper diameter of 40 µm was constructed. The taper diameter was smaller compared to the abrupt taper pair of diameter 68 µm. Two sensors comprising a gentle taper were fabricated and tested with configurations as follows:

1) Gentle taper (L_t = 20 mm, D_t = 35 µm) with abrupt taper pairs
2) Gentle taper (L_t = 50 mm, D_t = 40 µm) only

The findings showed that both configurations led to similar results, as opposed to the research findings of Tian (2008) in his thesis. Both sensors neither demonstrated a wavelength shift when refractive index of the surrounding liquid was increased, nor did the transmission spectra indicated any interference occurred between the core mode and cladding modes. However, for refractive index above that of the cladding, it was found that a power shift was obtained when the refractive index of the surrounding liquid changed.

Thus, it is strongly believed that the gentle taper sensor can be utilized for sensing refractive index, $n > n_2 = 1.453$ which posed as one of the limitations of an MZI sensor. In conclusion, further research in this direction can be done to realize a novel, high RI sensor.

REFERENCES

Chen, G. Y., Ding, M., Newson, T.P. and Brambilla G. (2013). A review of microfiber and nanofiber based optical sensors. The Open Optics Journal, 7, 32-57.

Chryssis, A.N., Lee, S.M., Lee, S.B., Saini, S.S. & Dagenais, M. (2005). High sensitivity evanescent field fiber Bragg grating sensor. IEEE Photonics Technology Letters, 17 (6), 1253-1255.

Dianov, E.M., Vasiliev, S.A., Kurkov, A.S., Medvedkov, O.I. & Protopopov, V.N. (1996). In-fiber Mach-Zehnder interferometer based on a pair of long-period gratings. Optical Communication, 1, 65-68.

Ding, J.F., Zhang, A.P., Shao, L.Y., Yan, J.H. & He S. (2005). Fiber-taper seeded long-period grating pair as a highly sensitive refractive-index sensor. IEEE Photonics Technology Letters, 17 (6), 1247-1249.

Fidanboylu, K. & Efendioglu, H.S. (2009). Fiber optic sensors and their applications. 5th International Advanced Technologies Symposium (IATS'09), May 13-15, Karabuk, Turkey.

Fu, H., Shu, X., Zhang, A., Liu, W., Zhang, L., He, S. & Bennion, I. (2011). Implementation and characterization of liquid-level sensor based on a long-period fiber grating Mach-Zehnder interferometer. IEEE Sensors Journal, 11 (11), 2878-2882.

Ghetia, S., Gajjar, R. & Trivedi, P. (2013). Classification of fiber optical sensors. International Journal of Electronics Communication and Computer Technology, 3 (4), 442-445.

Gouveia, C., Jorge, P.A.S., Baptista, J.M. & Frazao, O. (2012). Fabry-Pérot cavity based on a high-birefringent fiber Bragg grating for refractive index and temperature measurement. IEEE Sensors Journal, 12 (1), 17-21.

Iadicicco, A., Campopiano, S., Cutolo, A., Giordano, M. & Cusano, A. (2005). Refractive index sensor based on microstructured fiber Bragg grating. IEEE Photonics Technology Letters, 17 (6), 1250-1252.

Ji, W.B., Tjin, S.C., Lin, B. & Ng C.L. (2013). Highly sensitive refractive index sensor based on adiabatically tapered microfiber long period gratings. Sensors, 13, 14055-14063.

Kashyap, R. & Nayar, B.K. (1983). An all single-mode fiber Michelson interferometer sensor. Journal of Lightwave Technology, 1(4), 619-624.

Kheiri, M., Zibaii, M.I., Sadeghi, J. & Latifi H. (2011). Refractive index measurement by fat long period grating sensor on a single mode optical fiber. SPIE/OSA/IEEE, 8311, 83110B-1-83110B-6.

Liang, R., Sun, Q., Wo, J. & Liu, D. (2011). Theoretical investigation on refractive index sensor based on Bragg grating in micro/nanofiber. Photonics and Optoelectronics.

Liao, C.R., Wang, D.N., Wang, M. & Yang M. (2012). Fiber in-line Michelson interferometer tip sensor fabricated by femtosecond laser. IEEE Photonics Technology Letters, 24 (22), 2060-2063.

Liao, C.R., Wang, Y., Wang, D.N. & Yang, M.W. (2010). Fiber in-line Mach-Zehnder interferometer embedded in FBG for simultaneous refractive index and temperature measurement. IEEE Photonics Technology Letters, 22(22), 1686-1688.

Love, J.D., Henry, W.M., Stewart, W.J., Black, R.J., Lacroix, S. & Gonthier, F. (1991). Tapered single-mode fibres and devices: part 1 – adiabaticity criteria. IEEE Proceedings-J, 138 (5), 343-354.

Pang, F., Liu, H., Guo, H., Liu, Y., Zeng, X., Chen, N., Chen, Z. & Wang, T. (2011). In-fiber Mach-Zehnder interferometer based on double cladding fibers for refractive index sensor. IEEE Sensors Journal, 11(10), 2395-2400.

Shi, J., Xiao, S. & Bi, M. (2011). Sensitivity-enhanced refractive index sensor by using tapered thin-core fiber based inline Mach-Zehnder interferometer. PROC. SPIE 8311, Optical Sensors and Biophotonics III, 83110C.

Silva, C., Coelho, J.M.P., Caldas, P. & Jorge, P. (2012). Fibre sensing system based on long-period gratings for monitoring aqueous environments. Fiber Optic Sensors. InTech, 317-342.

Tian, Z.B. (2008). In-line optical fiber interferometric refractive index sensors. Master thesis. Queen's University.

Tian, Z.B. (2009). In-line optical fiber interferometric refractive index sensors. Journal of Lightwave Technology, 27 (13), 2296-2306.

Wang, X. (2012). Characterization of fiber tapers for fiber devices and sensors. Ph.D thesis, University of Ottawa.

Yu, H., Xiong, L., Chen, Z., Li, Q., Yi, X., Ding, Y., Wang, F., Lv, H. & Ding, Y. (2014). Ultracompact and high sensitive refractive index sensor based on Mach-Zehnder interferometer. Optics and Lasers in Engineering, 56 (2014), 50-53.

Zhu, T., Rao, Y.J., Wang, J.L. & Song Y. (2007). A highly sensitive fiber-optic refractive index sensor based on an edge-written long-period fiber grating. IEEE Photonics Technology Letters, 19 (24), 1946-1948.

Zhu, T., Song, Y. Rao, Y. & Zhu, Y. (2009). Highly sensitive optical refractometer based on edge-written ultra-long-period fiber grating formed by periodic grooves. IEEE Sensors Journal, 9 (6), 678-681.

APPENDICES

APPENDIX A: Graphs

For the first set of refractive index values which is 1.40-1.42, the corresponding spectral responses are shown as follows. The transmission spectra for all refractive indices showed an interference pattern between the core mode and the cladding modes indicated by the high extinction ratio. Due to such interference, wavelength shift and free spectral range shift were induced when the refractive index was changed

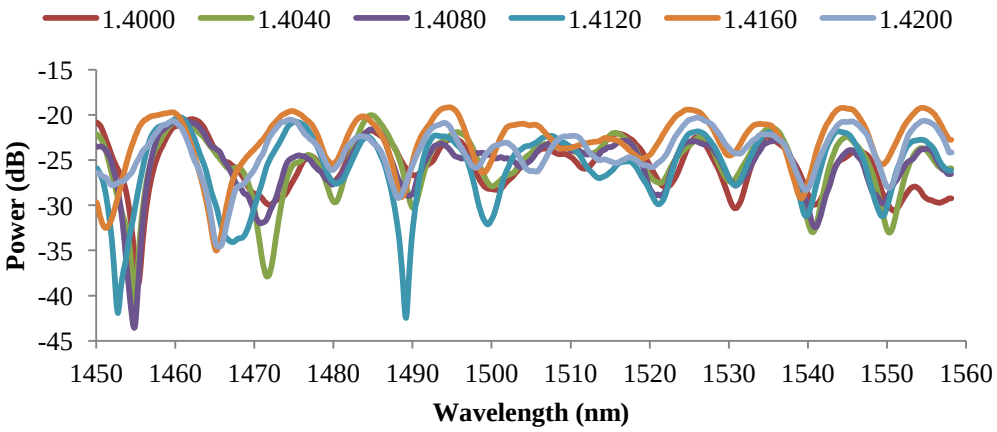

Figure A.1: Transmission spectra for refractive index 1.40-1.42.

.

The spectral responses for the second set of refractive index values are shown as follows. The transmission spectra for values equal to and below 1.44 showed clear interference pattern between the core mode and the cladding modes. As a result, characterization of the fiber sensor according to the wavelength shift and the free spectral range shift can be done.

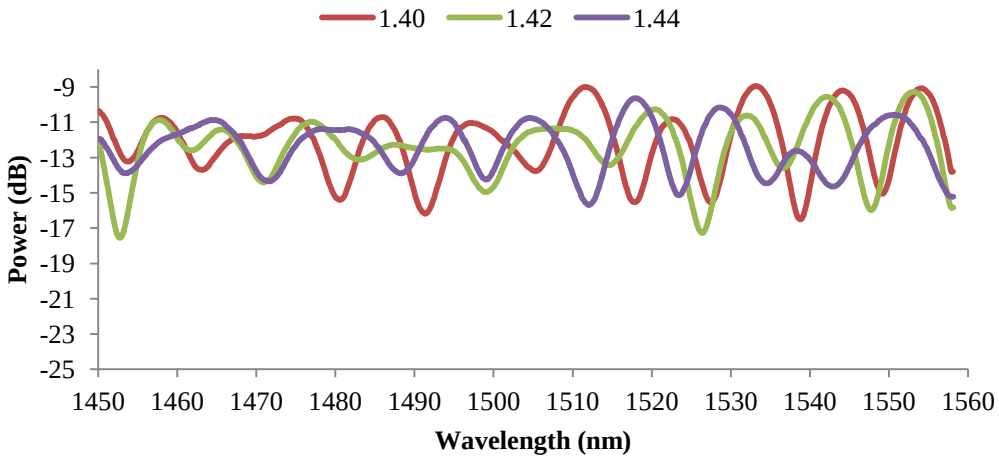

Figure A.2: Transmission spectra for refractive index 1.40-1.44.

The transmission spectra for values above 1.44 showed no interference between the core mode and the cladding modes. Due to a larger cladding refractive index, most of the light was not confined within the fiber but lost to the surrounding, thus cannot be detected by the spectrum analyser.

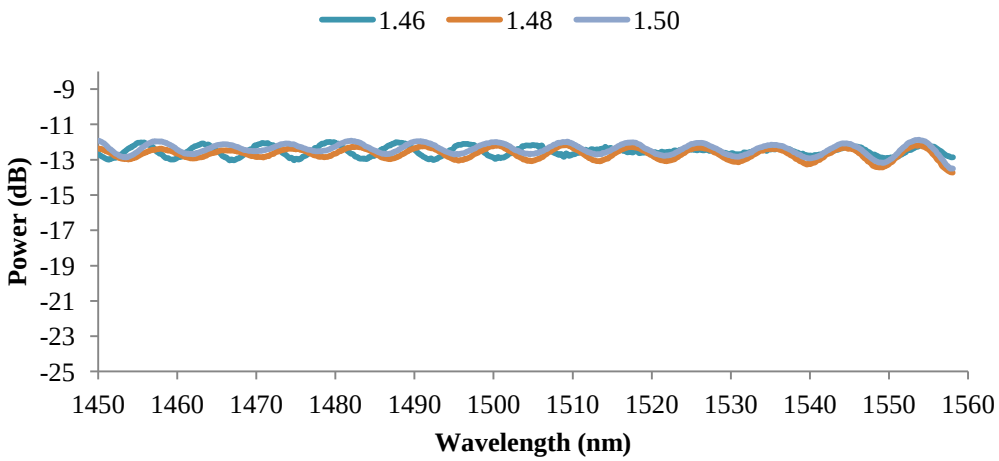

Figure A.3: Transmission spectra for refractive index 1.46-1.50.

In Chapter 5, an adiabatic taper with abrupt taper pair was mentioned. Its transmission spectra shows no light interference, however, there exists a power shift when RI changes.

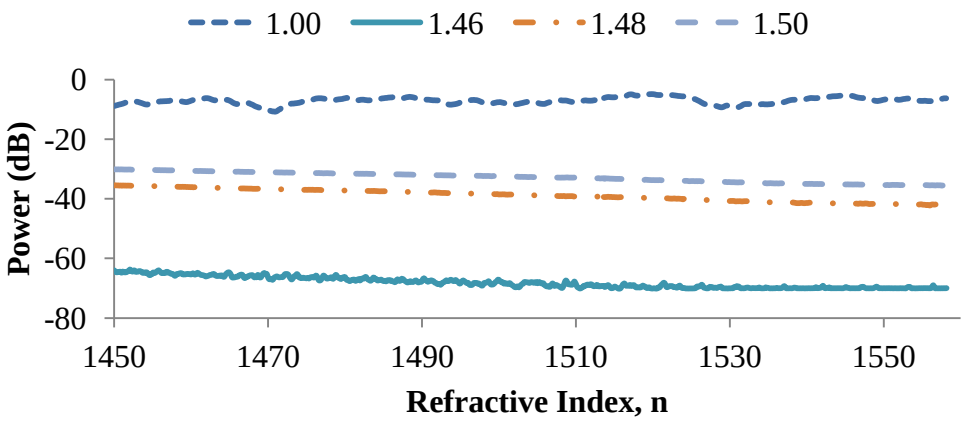

Figure A.4: Spectral Response for $n > n_2$.